Dosimetry of an Iodine-123-Labeled Tropane to Image Dopamine Transporters

P. David Mozley, James B. Stubbs, Hee-Joung Kim, Will McElgin, Mei-Ping Kung, Sanath Meegalla and Hank F. Kung
Division of Nuclear Medicine, University of Pennsylvania, Philadelphia, Pennsylvania; and Oak Ridge Institute for Science and Education, Oak Ridge, Tennessee

N-(3-Iodopropen-2-yl)-2β-carbomethoxy-3β-(4-chlorophenyl)tropane (IPT) is an analog of cocaine that selectively binds the presynaptic dopamine transporter. The present study sought to measure the radiation dosimetry of IPT in seven healthy human volunteers. **Methods:** Dynamic renal scans were acquired immediately after the intravenous administration of 165 ± 16 MBq (4.45 ± 0.42 mCi) of [^{123}I]IPT. Between 7 and 12 sets of whole-body scans were acquired over the next 24 hr. The 24-hr renal excretion fractions were measured from conjugate emission scans of 7–11 discreet voided urine specimens. The fraction of the administered dose in 11 organs and each urine specimen was quantified from the attenuation-corrected geometric mean counts in opposing views. Subject-specific residence times were calculated for each subject independently by fitting the time-activity curves to a multicompartmental model. The radiation doses were estimated with the MIRD technique from the residence times for each subject individually before any results were averaged. **Results:** The findings showed that IPT was excreted rapidly by the renal system. There were no reservoirs of retained activity outside the basal ganglia, where SPECT images in these subjects showed that the mean ratio of caudate to calcarine cortex averaged 25:1 at 3 hr after injection (range 19.6–32 hr). The basal ganglia received a radiation dose of 0.028 mGy/MBq (0.10 rad/mCi). The dose-limiting organ in men was the stomach, which received an estimated 0.11 mGy/MBq (0.37 rad/mCi). In women, the critical organ was the urinary bladder at 0.14 mGy/MBq (0.51 rad/mCi). **Conclusion:** Relatively high-contrast images of the presynaptic dopamine transporters in the basal ganglia can be acquired with 185 MBq (5 mCi) of [^{123}I]IPT. The radiation exposure that results is significantly less than the maximum allowed by current safety guidelines for research volunteers.

Key Words: dosimetry; dopamine transporter; iodine-123-tropane; SPECT

J Nucl Med 1996; 37:151–159

The reuptake of free dopamine from the synaptic cleft is mediated by a macromolecular transporter embedded in the axonal membrane (*1*). Cocaine (*2*) and some of its tropane derivatives block the transporter's dopamine reuptake sites (*3,4*). N-(3-Iodopropen-2-yl)-2β-carbomethoxy-3β-(4-chlorophenyl)tropane (IPT) has a binding affinity (K_d) of 0.2 n*M* for the dopamine transporter in vitro (*5*). The ratio of striatal to cerebellar uptake of IPT at 1 hr after intravenous injection has averaged 13.1:1 in anesthetized rats (*6*). Preclinical studies in nonhuman primates with SPECT have produced contrast ratios of basal ganglia to occipital lobe that averaged 22.8:1 at 3 hr after administration (*7*). Dynamic SPECT scans in monkeys have demonstrated that indirectly acting dopaminergic drugs decrease its uptake and increase its rate of elimination in the basal ganglia, whereas postsynaptic dopamine receptor antagonists do not (*7*). Displacement studies performed by following the administration of IPT with injections of monoamine-reuptake blocking agents, such as mazindol, GBR-12909 and beta-CIT (RTI-55), have shown that the binding is competitive and reversible. These findings have suggested that IPT may have several highly advantageous imaging characteristics for visualizing the dopamine transporter in dynamic SPECT studies that require high count rates and contrast ratios to achieve good temporal resolution. Estimates of the radiation dosimetry associated with IPT in a nonhuman primate were favorable (*8*) and led to the present study of its radiation dosimetry in healthy human volunteers. The protocol was designed to estimate the amount of radiation energy that would be deposited in each organ per unit dose of administered activity (*9*) (Fig. 1).

Received Oct. 20, 1994; revision accepted May 15, 1995.
For correspondence or reprints contact: P. David Mozley, MD, 110 Donner Bldg., Hospital of the University of Pennsylvania, 3400 Spruce St., Philadelphia, PA 19104.

MATERIALS AND METHODS

Subjects

The study protocol was approved by the local Human Subjects Committee (Institutional Review Board) and the Radioactive Drug Research Committee. Healthy volunteers were recruited through advertisements in local papers and by word of mouth. None of the participants were associated with the investigators or affiliated with the sponsoring university. Structured medical histories were taken, and physical examinations were performed. None of the volunteers had a health problem that could have significantly affected the biodistribution or elimination of the radioligand at the time of study, although one man had a past history of a single hospitalization for pneumonia. No subject had a history of a psychiatric disorder, although one had a brief course of couples therapy after his wife delivered a stillborn 2 yr before the study. No subject was taking any medication at the time of the study other than oral contraceptive pills.

Clinical laboratory screening-tests included a complete blood cell count with differential, serum electrolytes, liver enzymes and thyroid function tests. Serum cortisol and prolactin levels were assayed. Pregnancy was ruled out with measurements of serum beta-human choriogonadotropic levels. Routine urinalysis and urine toxicologic screening were performed after obtaining explicit consent for drug testing.

The final sample of seven subjects had a mean age of 28.8 ± 6.7 yr (range 19–42 yr). The five men had an average weight of 80.5 ± 9.1 kg (178.7 ± 20.3 lb) and a mean height of 180.1 ± 4.8 cm (70.9 ± 1.9 in.). The two women weighed an average of 50.5 ± 4.4 kg (112.2 ± 9.8 lb) and had a mean height of 161 ± 2.9 cm (63.4 ± 1.1 in.). All subjects had an average education of 14.7 ± 2.1 yr (range 12–20 yr).

Radionuclide

No-carrier-added sodium [^{123}I]iodide was obtained commercially (Nordion Intl., Kanata, Canada). It was produced with an enriched ^{124}Xe-labeled target. The principal contaminants were ^{121}Te (<0.05%), ^{124}I (<10^{-4}%), ^{125}I (<0.02%) and ^{126}I (<10^{-4}%) (Abeysekera B, *personal communication*, May 1993). The radionuclidic purity of each dose exceeded 99.8% at the time of delivery. Theoretically, the specific activity of the ^{123}I was 8.7 × 10^{18} Bq/mole (2.4 × 10^{8} mCi/mmole).

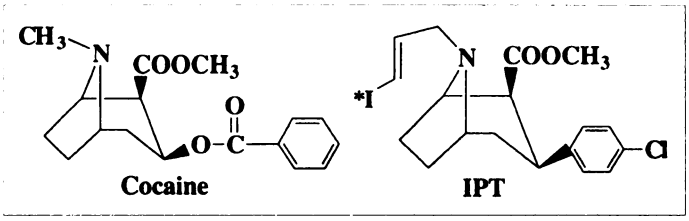

FIGURE 1. Chemical structures of cocaine and IPT.

Radiolabeling

The radiolabeling process began by adding 50 μl of 1 *N* hydrochloric acid to a shipping vial containing about 12 mCi sodium iodide. The acidified solution was transferred to a kit containing 50 μg of the lyophilized tributyl tin precursor dissolved in 50 μl ethanol. The iodination reaction was initiated by adding 50 μl of a 3% hydrogen peroxide solution and quenched 20 min later with 100 μl of a saturated sodium bisulfite solution. The solution was then neutralized with sodium bicarbonate and extracted with ethyl acetate three times. The combined extracts were passed through a column containing anhydrous sodium sulfate. The anhydrous ethyl acetate was condensed to dryness under a stream of nitrogen gas. The residue was redissolved in 100 μl ethanol and injected into a high-pressure liquid chromatographic (HPLC) system equipped with a PRP-1 reverse-phase column. The product was eluted with a mobile phase consisting of acetonitrile (pH 7.0) ammonium phosphate buffer (5 m*M*, 90:10). The fraction of the eluent corresponding to [^{123}I]IPT was separated and collected. Ascorbic acid (100 μg) was added as an antioxidant before the solution was condensed. The residue was then redissolved in 100 μl ethanol and diluted with 3 ml saline. The final solution was passed through a 0.22-μm filter before administration.

The final product was analyzed for purity by co-injecting a small portion into an HPLC column along with a standard solution of nonradioactive IPT. Analysis of the HPLC output was performed to measure the concordance between the elution of radioactivity and the ultraviolet peak for the parent chemical compound in the standard solution. Pyrogenicity tests were performed before administration. The unused portion of the final product was retained for sterility tests.

Measurements of Administered Activity

Measuring the fraction of the administered dose in each organ at each time point requires determining the total amount of injected activity. The present study analyzed conjugate images of the doses in their injection syringes to calculate the total amount of administered activity. The images were acquired while the injection syringes were lying on the imaging table both before and after administration with the same camera that was used to scan the subjects. The acquisition parameters were designed to match the corresponding images of the subjects, as shown in Table 1. The total amount of injected activity was calculated by subtracting the decay-corrected geometric mean number of counts in conjugate images of the injection syringe after administration from the geometric mean counts of the dose in the syringe before administration.

Measurements of Linear Attenuation

The number of counts in an emission image of an organ underestimates the true activity deposited in the organ because some of the emitted photons are absorbed by the surrounding tissues before striking the collimator, and others are scattered away from the collimator (*9,10*). The sum of photon absorbtion and scatter is defined as *attenuation*. Attenuation varies with the composition and the amount of tissue between the source organ and the collimator (*9*). The imaging table compounds the problem of attenuation even further in the posterior projection. The present study used transmission scans to correct for attenuation. An uncollimated transmission source was prepared by dissolving 150–300 MBq ^{123}I in a 1600-ml sheet flood made of lucite. The rectangular dimensions of the sheet flood were about the same size as the collimators on a dual-headed, whole-body camera. The flood was taped flat on top of the posterior projection collimator, which was always 43.5 cm from the surface of the anterior projection collimator on the upper head.

Nonattenuated scans of the transmission source were performed in the whole-body mode by acquiring images on the upper camera while the sheet source moved with it in tandem on the lower head. The scans were acquired for 10 min each over an excursion of 194 cm, which corresponded to 98 sec/pixel. The maximum speed at which the collimator traveled was less than 0.39 cm/sec, which tended to minimize fluid motion and maintain uniformity within the flood.

The imaging table was then replaced at a uniform height for all subjects, which was designed to place the midcoronal plane of an average adult in the center of the field between the two collimators. A whole-body transmission scan was then performed for 20 min (Fig. 2). The other acquisition parameters were identical to those that were used to acquire the nonattenuated transmission images of the flood and the subsequent emission scans (Table 1).

TABLE 1
Acquisition Parameters for Planar Images

	Injection syringes	Nonattenuated transmission	Transmission through subjects	Dynamic flow emission images	Whole-body emission scans	Voided urine specimens
Total duration	120 sec	10 min	20 min	2/8 min	20 min	120 sec
Time/per pixel	120 sec	98 sec	197 sec	2/30 sec	197 sec	120 sec
Pixel size	2.33 mm	2.18 mm	2.18 mm	2.33 mm	2.18 mm	2.33 mm
Matrix size	256 × 256	256 × 1024	256 × 1024	256 × 256	256 × 1024	256 × 256
Head radius	43.5 cm	43.5 cm	43.5 cm	43.5 cm	43.5 cm	43.5 cm
Excursion	None	194 cm	194 cm	None	194 cm	None
Maximum speed	NA	0.39 cm/sec	0.19 cm/sec	NA	0.19 cm/sec	NA

NA = not applicable.

FIGURE 2. Representative transmission and emission images of a 33-yr-old man. The ROIs for the bladder and stomach required constant operator interaction to compensate for normal changes in volume.

Emission Images

The sequence of measurements was designed to acquire the early emission images immediately after the transmission scans without moving the subject, so that the two sets of images would be optimally coregistered. The radiopharmaceutical was injected rapidly as a bolus through an indwelling catheter in an antecubital vein while dynamic images of the thorax and abdomen were acquired for 2 sec per frame for 60 frames in a 256 × 256 matrix. A series of static images were then acquired for 30 sec per frame for 16 frames without moving the collimators. These images were used to quantify the early time-activity curves for the kidneys. The first whole-body scan was begun 10 min after injection. Each whole-body scan was acquired in a 256 × 1024 matrix for 20 min over a total excursion length of 194 cm. The pixel size was 2.18 mm^2, which corresponded to a scanning time of 197 sec per pixel.

Each study began in the late afternoon near the end of the business day. The first five to nine whole-body scans were obtained during the next 5–7 hr. Delayed images were obtained the next morning between 13 and 16 hr after injection and the next evening between 23 and 26 hr after injection. A mean of nine whole-body images were acquired (range 7–12 images).

SPECT images of the brain were acquired for 30 min about 2.5 hr after injection on a triple-headed camera equipped with fan-beam collimators. The intrinsic resolution of the camera was rated at about 8–9 mm FWHM. The experimentally measured system resolution was 13 mm FWHM. The images were reconstructed with a count rate-dependent restoration filter. The modulation transfer function was generated from the line-spread function of the camera (*11*). The method of Chang et al. (*12*) was used to correct the SPECT scans for attenuation with a uniform ellipse.

Renal Excretion Fractions

Subjects were asked to micturate as often as possible during the first evening of study and collect their own urine overnight. If the time interval between voiding was less than 2 hr, the specimens were collected in 1200-ml containers. If the interval was more than 2 hr, a 5-liter container was used. The subjects produced an average of nine specimens (range 7–13 specimens) over 15–25 hr. Conjugate images of the urine specimens were acquired for 2 min in a 256 × 256 matrix by laying the samples out flat on the imaging table and scanning with the same acquisition parameters that were used to acquire the 256 × 256 static images of the injection syringes containing the administered doses. Checks were performed by measuring the volume of urine in each specimen and the activity in a 20-ml aliquot in the same well counter that was used to measure the injection syringes. The counts, however, in the conjugate images of specimens were used in the analyses.

Image Analysis

The images were exported to a graphics workstation (Sun Microsystems, Mountain View, CA). The image analysis package automatically measured the total number of counts in each 256 × 1024 image. An operator drew regions of interest (ROI) around 11 different organs, the whole-body and an off-body portion of the imaging table. The regions were drawn on whichever scan showed the organ most clearly after magnifying the image two to five times to facilitate tracing. Most organ boundaries were placed on the first whole-body scan, but the thyroid and stomach were always better visualized on the later images. Regardless of which scan the ROI originated from, it was cut and pasted into a single master set. Once the set was complete, the ROIs were transposed onto all the other images, including the transmission scans through the air and the subject. It was occasionally necessary for an operator to move the entire set of ROIs as a single unit to correct for small repositioning errors between scans. It was also necessary to periodically adjust the size of the ROIs for viscus organs, such as the stomach and urinary bladder, to account for normal changes in volume. Otherwise, the individual ROIs were rarely manipulated independently of the other regions in the set. An automated subroutine measured the number of counts in these ROIs. A representative example is shown in Figure 2.

Calculating Activity in an Organ

The transmission-corrected geometric mean number of counts in conjugate images of a point source is independent of its depth within an attenuating media and the thickness of the attenuating media along a line perpendicular to the collimator surfaces through the point source (*13,14*). Similarly, the process of calculating the activity in the injection syringes, the urine specimens and the ROIs for each source organ began by correcting the counts for decay and normalizing for unit time. Transmission-based attenuation corrections were then performed by multiplying the counts in each view of an organ by the number of counts per unit time in the same ROI on the nonattenuated image and dividing by the number of counts in the ROI for the organ on the transmission scan through the subject and table. Geometric means for each pair of transmission corrected conjugate ROIs were calculated by multiplying the anterior counts by the posterior counts and taking the square root of the product. The fraction of the injected dose at each time point was then estimated by dividing the corrected geometric mean number of counts in each ROI or urine specimen by the net geometric mean number of counts in the injection syringe, as shown in Equations 1 and 2:

$$C_{i\,(t)} = \frac{\sqrt{(C_{a.ROI} \times D_{f(t)}) \times (C_{p.ROI} \times D_{f(t)})}}{C_{t.subj}/C_{t.air}}, \qquad \text{Eq. 1}$$

$$C_{net.dose}$$

where $C_{i(t)}$ is the fraction of the administered dose in a given ROI at time t; $C_{a.ROI}$ is the anterior view count rate in the ROI at time t (in counts per minute); $C_{p.ROI}$ is the posterior view count rate in the ROI at time t (in counts per minute); $C_{t.air}$ is the counts in the ROI on the nonattenuated images of the flood (in counts per minute); $C_{t.subj}$ is the counts in the ROI on the transmission scan through the subject (in counts per minute); $D_{f(t)}$ is the decay factor for time t, where $D_{f(t)} = \exp[\ln(2) \times (t/13.2)]$; and $C_{net.dose}$ is the net counts in the conjugate images of the injection syringes (in counts per minute), equal to

$$\sqrt{(C^0_{a.dose} \times C^0_{p.dose})} - \sqrt{(C'_{a.dose} \times D_{f(t_d)})(C'_{p.dose} \times D_{f(t_d)})}, \qquad \text{Eq. 2}$$

where C^0 is the counts in the injection syringe containing the administered dose (in counts per minute); C' is the residual counts in the injection syringe after administration (in counts per minute); and $D_{f(t_d)}$ is the decay factor for the residual dose left in the injection syringe.

Checks were performed by adding the fraction of the dose in the ROI representing the whole field of view to the fraction of the dose excreted in the urine up to that time and comparing the sum with the net counts in the injection syringes or the total number of counts in the first set of emission images.

Organ Residence Times

Time-activity curves were generated directly from the experimental data for the brain, basal ganglia, genitalia, heart, kidney, liver, right lung, salivary glands, stomach, thyroid and the whole abdominal compartment, excluding the liver and the urinary bladder. The experimental data for these organs and were fitted with a multicompartmental model that was developed specifically to estimate organ residence times from the experimental data (Fig. 3). The model included nine other tissues that could not be measured directly on the images, such as the adrenal glands and bone marrow. The Simulation Analysis and Modeling (SAAM, Resource Facility for Kinetic Analysis, Seattle, WA) software that was used to mathematically fit the experimental data to the multicompartmental model has been described elsewhere (*15–19*). The model did not make any assumptions about the mechanism of IPT metabolism or its pharmacokinetic behavior other than its tissue distribution and excretion pathways.

The experimental measurements of urine activity were used to model the urinary excretion rates. The residence times for the urinary bladder and, thus, the dosimetric estimates that followed, were based on a theoretical bladder-voiding interval of 4.8 hr, or five times a day (*20*).

Activity that was not excreted in the urine was assumed to be eliminated in the feces. All the counts in the ROIs for the stomach were assumed to come from activity within the stomach wall. The activity in the bowel was assumed to be transferred through the alimentary canal according to the kinetic model for the gastrointestinal tract in *ICRP Publication 30* (*21*). The standard mass of tissue in each region of the gut was taken from *ICRP Publication 23* (*22*).

The residence times were used to estimate the absorbed doses with the MIRD technique (*23*). For calculations in men, the mass of the organs and their spatial relationships with the other bodily tissues were based on the (American) Adult Reference Man (*24,25*). This model is based on a height of 175 cm (5 ft 7 in.) and a weight of 75 kg (152 lb). To prevent the absorbed doses from being underestimated in women by assuming that the measured activity was distributed in a reference body that was 28% larger than the mean body weight in the sample, the calculations for the female subjects were based on the Adult Reference Woman (*23*). The organ doses were calculated for each subject individually before the results were averaged.

RESULTS

There were no subjective effects of the radiotracer on any of the volunteers. Their vital signs remained stable throughout the procedure, and there were no changes observed on physical examination. There were no meaningful changes in any of the clinical laboratory assays that were performed 24 hr after the administration of the tracer.

The mean dose of [^{123}I]IPT administered in the present study was 178 MBq (4.81 mCi) (range 159–189 MBq [4.30–5.11 mCi]). Images of the administered doses in their injection syringes contained a mean ± s.d. of 684,000 ± 69,000 net cpm (range 512,000–755,000 cpm). Concomitantly performed calibration studies showed that this count rate was well within the linear response range of both cameras. Retrospectively pooling the data from both cameras showed that the correlation coefficient r describing the relationship between the seven measured doses and the corresponding camera counts was 0.985 in this sample. Most of the variation could be accounted for by the slightly different response characteristics of the two identical cameras that were used. The difference, however, was not a factor in this study because the subjects were always imaged on the same camera that was used to scan their doses.

The nonattenuated images of the transmission source contained a mean of 3.40 million counts (range 2.16 to 4.45 million counts). Grid analysis of the actual data over the useful field of view showed that the count rates in approximately 1000-pixel boxes had an internal standard deviation that was always less than 10%. The variance between different regions of the field was always less than 10%. The transmission scans through the subjects, which were acquired for twice as long as the nonattenuated images, contained similar numbers of counts in the whole field of view. The magnitude of the linear attenuation correction factors varied. Only 13.1% ± 3.2% of the counts from the flood were transmitted through the liver plus the imaging table, whereas an average of 23.8% ± 4.3% passed through the lungs plus the imaging table. The greatest intersubject variability was found in the ROI for the whole abdomen,

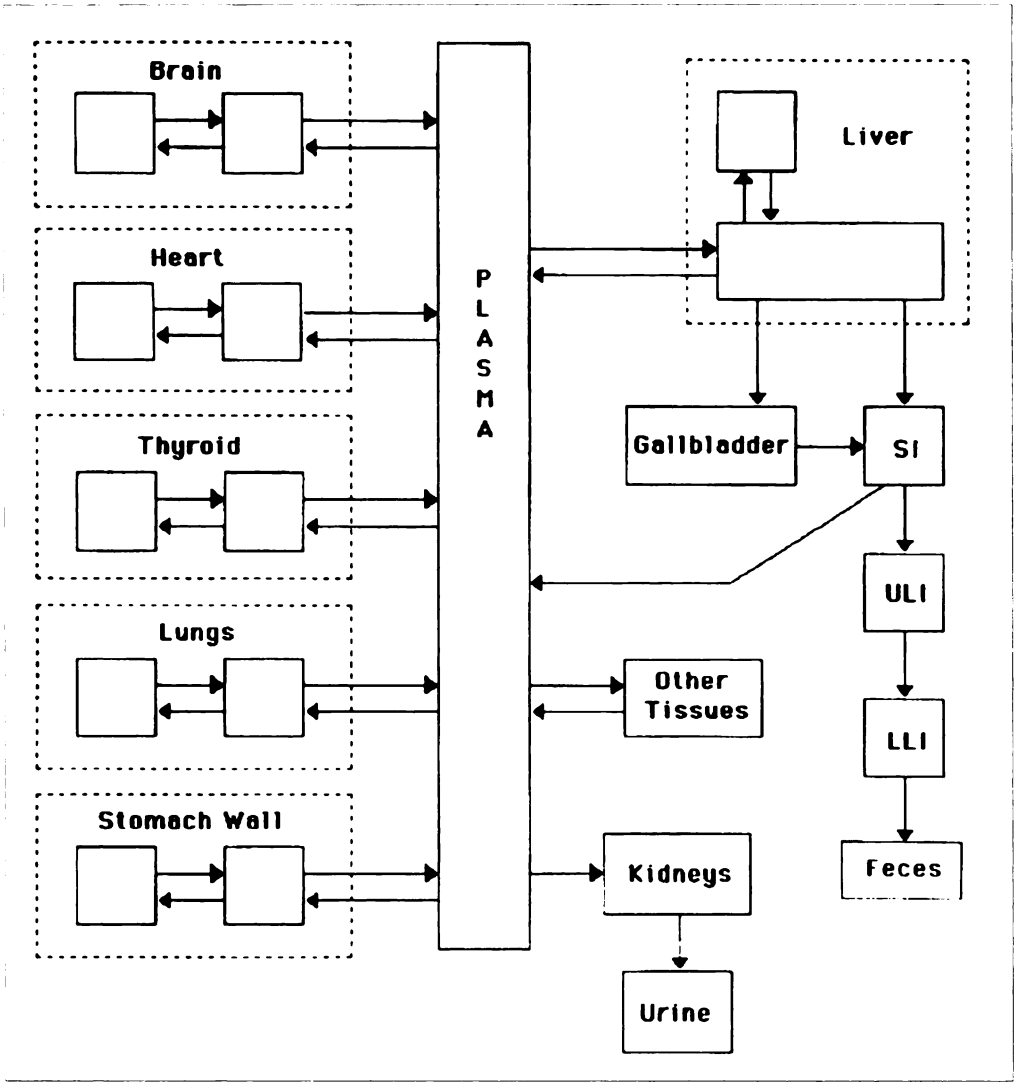

FIGURE 3. Compartmental model used to fit the time–activity curves in each subject individually. SI = small intestine; ULI = upper large intestine; LLI = lower large intestine.

where the standard deviation was 25.9% of the mean value. The least variability was found in the ROI for the basal ganglia, where the standard deviation was 12.3% of the mean value.

The sum of the attenuation corrected counts in the 256 × 1024 emission images plus the activity already voided in the urine never deviated by more than 3% from the total number of transmission corrected counts in the initial set of emission images during the first 16 hr of study. As time progressed, the number of counts that could be recovered from all sources of activity appeared to increase to more than 110% of the total injected activity.

A review of the images showed that there were no reservoirs of retained activity outside the basal ganglia in any of the subjects. The radioactivity associated with IPT was cleared from the blood and the ROI for the whole heart within minutes of administration. Activity was taken up by the liver rapidly, but there was no visual evidence to suggest that much of it was excreted in the bile. Activity was never visualized in the billiary tree or gallbladder. The concentration of IPT in the liver peaked on the first emission image 10–30 min after injection. Hepatic activity could rarely be visualized after 1 hr without brightening the images significantly. Large-bowel patterns were never visualized on the images.

Image analysis demonstrated that the radioactivity associated with IPT was excreted by the renal system. The activity in the kidneys peaked 5.5 ± 1.5 min after injection (range 4.5–7.0 min) at a mean of 5.2% ± 0.7% of the injected dose (range 3.9%–7.5%). Image analysis of the urine specimens produced experimentally measured renal excretion fractions of 53.4%–79.7% during the first 16 hr, with a mean of 76% by 16 hr.

In contrast to the findings in nonhuman primates, activity could not be visualized in the heart on any of the whole-body images. Analysis of the dynamic scans that were acquired immediately after injection was not indicative of any myocardial retention. The heart could not be visualized on SPECT scans of the chest that were performed 30 min after administration in a 19-yr-old man who was tall and thin.

The basal ganglia could be distinguished from the rest of the brain on the first set of planar scans, which began 10 min after administration (Fig. 2). SPECT images of the brain in these relatively young dosimetric subjects produced contrast ratios of caudate to calcarine cortex that averaged 25.6:1 approximately 2.5 hr after administration (range 19.1–31.0 hr). The high contrast on the SPECT images tended to confirm that the intact tracer crosses the blood-brain barrier easily in humans (Fig. 4). Comparisons between the IPT-SPECT images and SPECT images made with other dopaminergic tracers in four of these subjects showed a high degree of concordance and indicated that IPT is selective for dopaminergic regions of the brain in humans.

Calculations of the residence times for each subject individually before the results were averaged showed that the effective half-life of radioactivity associated with IPT was longest in the

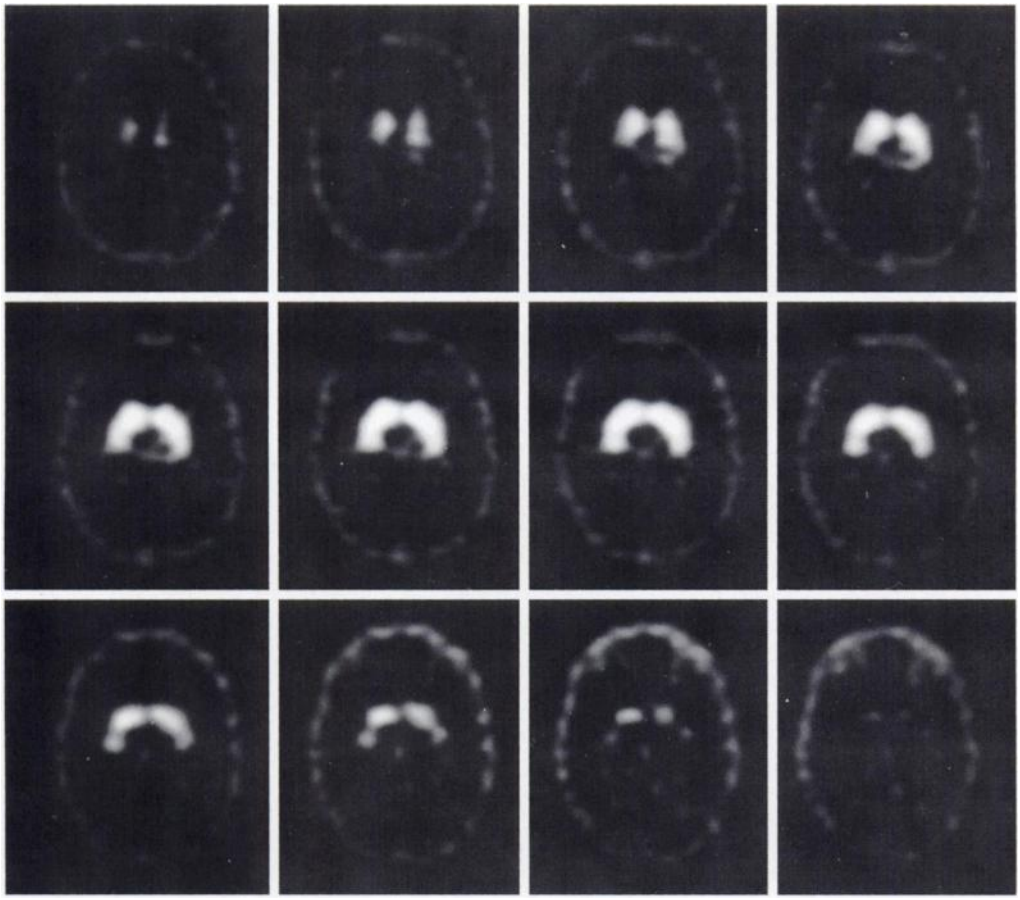

FIGURE 4. SPECT scan of the brain acquired 2.5 to 3 hr after administration. The brightness had to be increased significantly to show the faint activity in the bone marrow of the skull.

lungs at 1.33 hr (range 1.11–1.79 hr), followed by the urinary bladder (1.18 hr) and the liver (1.00 hr). Table 2 shows the mean, minimum and maximum organ residence times for men and women. The minimum and maximum times represent the most extreme values calculated in any single subject before the results were averaged. The percent standard deviation (PSD) was calculated to compare the variability in the present study with that from similar investigations. The PSD was defined as the ratio of the standard deviation to the mean organ dose and ranged from 5% in the urinary bladder to 56% in the thyroid. The mean PSD in the organs that could be measured directly on the images was 19%.

TABLE 2
Residence Times for Iodine-123 Activity after IPT Injection

	Men				Women			
Organ	Mean (hr)	Min (hr)	Max (hr)	PSD (%)	Mean (hr)	Min (hr)	Max (hr)	PSD (%)
Remainder of body	3.34	1.96	4.71	36	3.81	3.37	4.25	16
Lungs	1.32	1.11	1.79	21	0.85	0.57	1.14	47
Urinary bladder contents	1.17	1.09	1.24	5	1.19	1.14	1.24	6
Liver	1.03	0.80	1.26	19	0.95	0.92	0.97	3
Stomach wall	0.81	0.36	1.38	51	0.90	0.53	1.27	58
Kidneys	0.72	0.14	1.48	68				
Upper large intestine	0.54	0.33	0.74	28	0.48	0.37	0.58	31
Lower large intestine	0.43	0.26	0.59	28	0.38	0.30	0.46	31
Brain	0.39	0.32	0.47	16	0.35	0.30	0.40	21
Small intestine	0.28	0.17	0.38	28	0.24	0.19	0.30	30
Heart wall	0.25	0.19	0.34	26	0.28	0.24	0.32	19
Testes	0.18	0.06	0.36	60				
Gall bladder contents	0.07	0.04	0.10	29	0.07	0.05	0.08	23
Thyroid	0.05	0.03	0.08	42	0.10	0.07	0.13	45
Basal ganglia	0.03	0.02	0.04	29	0.03	0.03	0.04	29

Min = minimum; Max = maximum; PSD = percent standard deviation.

Table 3 shows the absorbed dose estimates for the study subjects. The organs of excretion and the tissues that ordinarily take up free iodide received the highest doses of radiation. There were several differences between men and women, but the bladder, kidneys, thyroid and stomach received the most radiation in both groups. The dose-limiting organ in men was the stomach, which received an estimated 0.11 mGy/MBq (0.37 rad/mCi), followed by the bladder, which received a dose of 0.097 mGy/MBq (0.36 rad/mCi). In women, the critical organ was the urinary bladder (0.14 mGy/MBq) followed by the stomach (0.13 mGy/MBq) and the thyroid (0.12 mGy/MBq). The effective dose equivalent (EDE) in men was 0.031 mSv/MBq (range 0.026–0.041 mSv/MBq). The EDE in women was 0.037 mSv/MBq (range 0.034–0.39 mSv/MBq).

TABLE 3
Dose Estimates for Iodine-123-IPT

	Men			
	Mean dose		Minimum	Maximum
Organ	mGy/MBq	rad/mCi	(mGy/MBq)	(mGy/MBq)
Stomach	1.1E-01	3.7E-01	5.2E-02	1.8E-01
Urinary bladder	9.7E-02	3.6E-01	8.6E-02	1.2E-01
Kidneys	7.7E-02	2.8E-01	1.8E-02	1.7E-01
Thyroid	5.6E-02	2.1E-01	4.0E-02	8.4E-02
Colon				
LLI	4.6E-02	1.7E-01	3.6E-02	5.7E-02
ULI	4.1E-02	1.6E-01	3.4E-02	5.1E-02
Lungs	4.1E-02	1.5E-01	3.2E-02	7.0E-02
Gallbladder	3.0E-02	1.1E-01	2.6E-02	3.5E-02
Heart	2.9E-02	1.1E-01	2.2E-02	4.5E-02
Basal ganglia	2.8E-02	1.0E-01	2.2E-02	4.2E-02
Liver	2.8E-02	1.0E-01	2.1E-02	4.1E-02
Small bowel	2.0E-02	7.4E-02	1.8E-02	2.3E-02
Pancreas	1.5E-02	5.6E-02	1.1E-02	1.9E-02
Adrenals	1.2E-02	4.4E-02	9.0E-03	1.8E-02
Whole brain	1.2E-02	4.2E-02	1.0E-03	1.4E-02
Spleen	1.1E-02	4.2E-02	7.2E-03	1.5E-02
Bone surface	1.0E-02	3.7E-02	8.5E-03	1.1E-02
Bone marrow	6.5E-03	2.4E-02	5.8E-03	6.9E-03
Muscles	6.5E-03	2.4E-02	5.7E-03	7.0E-03
Testes	5.4E-03	2.0E-01	4.4E-02	6.1E-01
Skin	3.3E-O3	1.2E-02	2.7E-03	3.8E-03
Uterus				
Ovaries				
Breasts				
Effective dose equivalent	3.1E-02 (mSv/MBq)	1.2E-01 (rem/mCi)	2.6E-02 (mSv/MBq)	4.1E-02 (mSv/MBq)

LLI = lower large intestine; ULI = upper large intestine.

DISCUSSION

Tracer amounts of IPT appear to be pharmacologically safe in healthy volunteers. High-resolution SPECT images of the basal ganglia could be acquired with 185 MBq (5 mCi) of no-carrier-added IPT without producing any subjective or objective side effects in any of the volunteers. The lack of an effect from administering less than 50 ng (10^{-9} g) of IPT is consistent with the observation that 50–200 mg cocaine are required to produce a pharmacological response (*26,27*).

The radiation dosimetric estimates for IPT appear favorable. Rapid elimination by the kidneys tends to minimize the radiation exposure to most organs. High-contrast SPECT images of the basal ganglia containing reasonably good counting statistics could be produced with significantly less than the maximum dose of [^{123}I]IPT recommended (*28*) or allowed (*29*) by current safety guidelines for research volunteers. The actual radiation doses are probably even lower than the estimates that were calculated in the present study because several features of the design (e.g., most of the assumptions made in modeling) were conservative.

One of the dose-limiting organs for both men and women was the urinary bladder, where the residence times were usually longer than in any other tissue. The estimate of 0.09–0.14 mGy/MBq (0.32–0.52 rad/mCi), however, was based on an even longer theoretical voiding interval of 4.8 hr, or five times a day. In clinical practice, the absorbed dose to the urinary bladder wall can probably be reduced substantially by encouraging subjects to micturate right after the neuroimaging procedure and voiding more than twice during the first 9 hr after administration like the model assumed.

Another dose-limiting organ in this group appeared to be the thyroid. Although some of the counts in the ROI for the thyroid may have actually come from the intact parent compound or its organic metabolites in the thyroid and underlying parathyroid glands, most of the activity was probably attributable to the uptake of free [^{123}I]iodide by the thyroid itself. The subjects in this sample were pretreated with a single, 67.5-mg dose of potassium iodide (KI) about 1 hr before administration. This is only 50% of the dose that is recommended to achieve a thyroid blockade of 95%–98% (*30*). In clinical practice, the uptake of free [^{123}I]iodide can probably be reduced with higher dosing regimens of KI.

Several of the assumptions that are inherent in the Reference Man led to an overestimation of the dosimetry in men. The (American) Adult Reference Man weighs 70 kg (*24*). The men in the present sample actually weighed an average of 80.5 ± 9.1 kg. The standard caused the dose estimates in men to be artifactually elevated because the reference assumed that the measured activity was distributed in disproportionately smaller masses of tissue. Reference Man is also shorter than the men in the present study, which inflated the estimates by assuming that the source organs were separated from one another by smaller distances than they actually were. In contrast, the women who participated in the present study only weighed a mean of 50.9 kg. The use of Reference Man to model their dosimetry would have artifactually lowered their estimates significantly (*31*). Even the Reference Woman model weighed about 9.1% more than the mean for the women who participated in the present study and still slightly underestimated their exposure. The heights of the model and the female subjects were comparable.

The dose estimates to the basal ganglia were less than the estimates for other ^{123}I-labeled radiopharmaceuticals for imaging the dopamine transporter. The uptake of IPT by the brain was rapid. The basal ganglia could be distinguished from the background in the rest of the brain on the very first set of planar images, which were performed only 10 min after injection. There was still enough activity in the basal ganglia to produce high-contrast images 3 hr after administration, but there was virtually no activity in the brain after 16 hr. These observations are consistent with the results of published studies in animals that showed that the binding of IPT to the transporter is competitive (*7,8*). A higher renal excretion fraction also seems to distinguish IPT from β-CIT, which is excreted primarily by the liver into the gastrointestinal tract (*32*). In contrast, the radioactivity associated with IPT was never visible in the bowel despite initially high uptake by the liver. Slower enteric excretion tends to make the residence times in most organs longer for β-CIT than they are for IPT. This may partially

TABLE 3
Dose Estimates for Iodine-123-IPT (Continued)

Women				Whole Sample			
Mean dose		Minimum	Maximum	Mean dose		Minimum	Maximum
mGy/MBq	rad/mCi	(mGy/MBq)	(mGy/Mbq)	mGy/MBq	rad/mCi	(mGy/MBq)	(mGy/MBq)
1.3E−01	4.9E-01	8.1E-02	1.8E-01	1.2E-01	4.0E-01	5.2E-02	1.8E-01
1.4E−01	5.1E-01	1.3E-01	1.4E-01	1.1E-01	4.0E-01	8.6E-02	1.4E-01
8.1E−02	3.0E-01	7.8E-02	8.3E-02	7.8E-02	2.9E-01	1.8E-02	1.7E-01
1.2E−01	4.6E-01	8.4E-02	1.6E-01	7.4E-02	2.8E-01	4.0E-02	1.6E-01
4.6E−02	1.7E-01	3.8E-02	5.3E-02	4.6E-02	1.7E-01	3.6E-02	5.7E-02
4.3E−02	1.6E-01	3.6E-02	4.9E-02	4.2E-02	1.6E-01	3.4E-02	5.1E-02
3.3E−02	1.2E-01	2.3E-02	4.2E-02	3.9E-02	1.4E-01	2.3E-02	7.0E-02
3.2E−02	1.2E-01	2.8E-02	3.5E-02	3.1E-02	1.1E-01	2.6E-02	3.5E-02
3.7E−02	1.4E-01	3.5E-02	3.9E-02	3.1E-02	1.2E-01	2.2E-02	4.5E-02
3.4E−02	1.3E-01	3.1E-02	3.7E-02	3.0E-02	1.1E-01	2.2E-02	4.2E-02
3.2E−02	1.2E-01	3.0E-02	3.3E-02	2.9E-02	1.1E-01	2.1E-02	4.1E-02
2.2E−02	8.2E-02	2.0E-02	2.4E-02	2.1E-02	7.6E-02	1.8E-02	2.4E-02
1.9E−02	6.9E-02	1.5E-02	2.2E-02	1.6E-02	6.0E-02	1.1E-02	2.2E-02
1.4E−02	5.3E-02	1.3E-02	1.5E-02	1.3E-02	4.7E-02	9.0E-03	1.8E-02
1.3E−02	4.5E-02	1.1E-02	1.4E-02	1.2E-02	4.3E-02	1.0E-03	1.4E-02
1.4E−02	5.1E-02	1.2E-02	1.6E-02	1.2E-02	4.5E-02	7.2E-03	1.6E-02
1.2E−02	4.6E-02	1.1E-02	1.3E-02	1.1E-02	4.0E-02	8.5E-03	1.3E-02
7.7E−03	2.9E-02	7.2E-03	8.1E-03	6.8E-03	2.5E-02	5.8E-03	8.1E-03
7.9E−03	2.9E-02	7.2E-03	8.5E-03	6.9E-03	2.5E-02	5.7E-03	8.5E-03
			5.4E-03	2.0E-02	4.4E-03	6.1E-03	
4.2E−03	1.6E-02	3.8E-03	4.6E-03	3.6E-03	1.3E-02	2.7E-03	4.6E-03
1.9E−02	6.8E-02	1.8E-02	1.9E-02	1.9E-02	6.8E-02	1.8E-02	1.9E-02
1.7E−02	6.4E-02	1.6E-02	1.8E-02	1.7E-02	6.4E-02	1.6E-02	1.8E-02
5.5E−03	2.0E-02	4.7E-03	6.2E-03	5.5E-03	2.0E-02	4.7E-03	6.2E-03
3.7E−02	1.4E-01	3.4E-02	3.9E-02	3.3E-02	1.3E-01	2.6E-02	4.1E-02
(mSv/MBq)	(rem/mCi)	(mSv/MBq)	(mSv/MBq)	(mSv/MBq)	(rem/mCi)	(mSv/MBq)	(mSv/MBq)

LLI = lower large intestine; ULI = upper large intestine.

explain why the IPT activity in the basal ganglia decreases with time, whereas the (decay corrected) activity of β-CIT increases with time (*33*).

The activity associated with IPT did not continuously accumulate in any tissue. The organs that normally take up free iodide initially took up relatively large amounts of the radioactivity associated with IPT. The slowest times to peak were in the stomach at about a mean of 2 hr, which caused the dose estimates for the stomach to be relatively high. The finding that the stomach is the dose-limiting organ tends to be corroborated by the observation that the gastric borders were so clearly visualized on the images, in marked contradistinction to several other radiopharmaceuticals that we have studied with the same protocol. The estimates, however, may still be somewhat inflated. The model assumed that all the gastric activity was free iodide within the mucosal cells themselves. Although contrary to established physiological mechanisms, it was assumed that no gastric activity was ever excreted into the lumen of the stomach.

The conservative set of assumptions about how activity in the ROI for the stomach was physiologically handled produced the highest dose estimate to a single organ in the sample of 0.18 mGy/MBq (0.67 rad/mCi). If the dose of IPT were limited by the worst case in any organ from a single outlier, then 280 MBq (7.5 mCi) would still conform to current safety guidelines for research volunteers. Using the mean value of 0.11 mGy/MBq (0.37 rad/mCi) for the critical organ would allow 500 MBq (13.5 mCi) to be administered.

CONCLUSION

Our findings indicate that IPT may be a useful imaging agent for studying the presynaptic dopamine transporter with dynamic SPECT protocols that require relatively rapid acquisition times and high target-to-background contrast ratios.

ACKNOWLEDGMENTS

This study was partially supported by National Institutes of Health grant NS-24538 and National Institute of Mental Health grant MH-43880. The clinical laboratory studies performed by the General Clinical Research Center at the University of Pennsylvania Medical Center were made possible by National Institutes of Health grant MO1-RR00040. The services by the Oak Ridge Institute for Science and Education were performed under Interagency Agreement No. FDA 224-75-3016 and DOE 40-286-71.

REFERENCES

1. Cooper JR, Bloom FE, Roth RH. *The biological basis of neuropharmacology.* 6th ed. New York: Oxford University Press; 1991:292–294.
2. Johanson CE, Fischman M. The pharmacology of cocaine related to its abuse. *Pharmacol Rev* 1989;41:3–52.
3. Carroll FI, Abram P, Lewin AH, Parham K, Boja JW, Kuhar MJ. Isopropyl and phenyl esters of 3b-(4-substituted phenyl)tropan-2b-carboxylic acids: potent and selective compounds for the dopamine transporter. *J Med Chem* 1992;35:2497–2500.
4. Madras B, Spealman R, Fahey M, Neumeyer J, Saha J, Milius R. Cocaine receptors labeled by [3H]2b-carbomethoxy-3b-(4-fluorophenyl)tropane. *Mol Pharmacol* 1989; 36:518–524.
5. Kung M-P, Essman WD, Frederick D, et al. IPT: a novel iodinated ligand for the CNS dopamine transporter. *Synapse* 1995;20:316–324.
6. Goodman MM, Mung M-P, Kabalka GW, Kung HF, Switzer R. Synthesis and characterization of radioiodinated N-(3-Iodopropen-1-yl)2B-carbomethoxy-3B-(4-

chlorophenyl) tropanes: potential dopamine reuptake site imaging agents. *J Med Chem* 1994;37:1535–1542.
7. Malison RT, Vessotskie J, Kung M-P, et al. SPECT imaging of striatal dopamine transporters in non-human primates with [I-123]IPT. *J Nucl Med* 1995;36:2290–2297.
8. Mozley PD, Kim H-J, Stubbs JB, et al. Brain and cardiac uptake of I-123 IPT: an analog of cocaine [Abstract]. *J Nucl Med* 1994;35(suppl):129P.
9. Sorenson JA, Phelps ME: *Internal radiation dosimetry*. In: *Physics in nuclear medicine*, 2nd ed. Philadelphia: W.B. Saunders; 1987:197–218.
10. Budinger TF, Gullberg GT, Huesman RH. Emission computed tomography. In: Herman GT, ed. *Image reconstruction from projections*. Berlin: Springer-Verlag; 1979:147–242. (*Topics in Applied Radiology; vol. 32).*
11. Kim H-J, Karp JS, Kung HF, Mozley PD. Quantitative effects of a count rate dependent Wiener filter on image quality: a basal ganglia phantom study simulating ^{123}I dynamic SPECT imaging [Abstract]. *J Nucl Med* 1993;34(suppl):190.
12. Chang LT. A method for attenuation correction in radionuclide computed tomography. *IEEE Trans Nucl Sci* 1978;NS-25:638–643.
13. Jones JP, Brill AB, Johnson RE. The validity of an equivalent point source assumption used in quantitative scanning. *Phys Med Biol* 1975;20:455–464.
14. Thomas SR, Maxon HR. In vivo quantitation of lesion radioactivity using external counting methods. *Med Phys* 1976;3:253–255.
15. Robertson J. *Compartmental distribution of radiotracers*. Boca Raton, FL: CRC Press; 1983.
16. Stubbs JB, Smith GT, Stabin MG, Eckerman KF, Turner JE. An approach to cellular level dosimetry using compartmental model analysis and dynamic PET. Watson EE, Schlafke-Stelson A, *eds. Proceedings of the fifth international symposium on radiopharmaceutical dosimetry.* May 1991;385–395.
17. Stabin M, Taylor A Jr, Eshima D, Wooter W. Radiation dosimetry for technetium-99m-MAG3, technetium-99m-DTPA and iodine-131-OIH based on human biodistribution studies. *J Nucl Med* 1992;33:33–40.
18. Mozley PD, Stubbs JS, Kung HF, Selickson MH, Stabin MG, Alavi A. Biodistribution and Dosimetry of I-123 IBF: a potent radioligand for imaging the D2 dopamine receptor. *J Nucl Med* 1993;34:1910–1917.
19. Mozley PD, Stubbs JB, Kim H-J, et al. Biodistribution and dosimetry of a D2/D3 dopamine receptor antagonist that can be used with either PET or SPECT. *J Nucl Med* 1995;35:1322–1331.
20. Cloutier RJ, Smith SA, Watson EE, Snyder WS, Warner GG. Dose to the fetus from radionuclides in the bladder. *Health Phys* 1973;25:147–161.
21. International Commission on Radiation Protection. *ICRP publication 30. Limits for intake of radionuclides by workers*. New York: Pergamon Press; 1979.
22. International Commission on Radiation Protection. *ICRP publication 23. Report of the task group on reference man*. Oxford: Pergamon Press; 1979.
23. Loevinger R, Berman M. *A revised schema for calculating the absorbed dose from biologically distributed radionuclides. MIRD pamphlet no. 1* (revised). New York: Society of Nuclear Medicine; 1975.
24. Cristy M, Eckerman K. *Specific absorbed fractions of energy at various ages from internal photon sources*. Oak Ridge, TN: ORNL/TM-8381: 1987.
25. Snyder WS, Ford MR, Warner GG, Watson SB. *"S" absorbed dose per unit cumulated activity for selected radionuclides and organs. MIRD pamplet no. 11*. New York: Society of Nuclear Medicine; 1975.
26. Lange RA, Cigarroa RG, Yancey CW Jr, et al. Cocaine-induced coronary-artery vasoconstriction. *N Engl J Med* 1989;321:1157–1162.
27. Moliterno DJ, Willard JE, Lange RA, et al. Coronary-artery vasoconstriction induced by cocaine, cigarette smoking, or both. *N Engl J Med* 1994;330:454–459.
28. National Council of Radiation Protection and Measurements. *NCRP report No. 39, Basic Radiation Protection Criteria*. Washington D.C.: National Council of Radiation Protection and Measurements; 1971.
29. Food and Drug Administration, HHS: Radioactive drugs for certain research uses. Code of Federal Regulations (CFR) 21, Ch. 1 (4-1-89 Edition), Part 361.1, paragraph (b) (3) (i), p. 206.
30. National Council on Radiation Protection and Measurement (NCRP). *Protection of the thyroid gland in the event of releases of radioiodine*. Washington, D.C.: NCRP report no. 55, August 1, 1977.
31. Mejia AA, Nakamura T, Masatoshi I, Hatazawa J, Masaki M, Watanuki S. Estimation of absorbed doses in humans due to intravenous administration of fluorine-18-fluorodeoxyglucose in PET studies. *J Nucl Med* 1991;32:699–706.
32. Kuikka JT, Bergstrom KA, Ahonen A, Lansimies E. The dosimetry of iodine-123 labelled 2-carbomethoxy-3-(4-iodophenyl)tropane. *Eur J Nucl Med* 1994;21:53–56.
33. Neumeyer JL, Wang S, Milius RA, et al. [123I]-2b-Carbomethoxy-3b-(4-iodophenyl)tropane: high-affinity SPECT radiotracer of monoamine reuptake sites in brain. *J Med Chem* 1991;34:3144–3146.